JOURNAL OF AGRICULTURAL AND FOOD CHEMISTRY

Article

Synthesis and crystal structure of new Temephos analogous as cholinesterase inhibitor: molecular docking, QSAR study and hydrogen bonding analysis of solid state

Khodayar Gholivand, Ali Asghar Ebrahimi Valmoozi, and Mahyar Bonsaii

J. Agric. Food Chem., **Just Accepted Manuscript** • DOI: 10.1021/jf5011726 • Publication Date (Web): 03 Jun 2014

ACS Publications
High quality. High impact.

Journal of Agricultural and Food Chemistry is published by the American Chemical Society. 1155 Sixteenth Street N.W., Washington, DC 20036

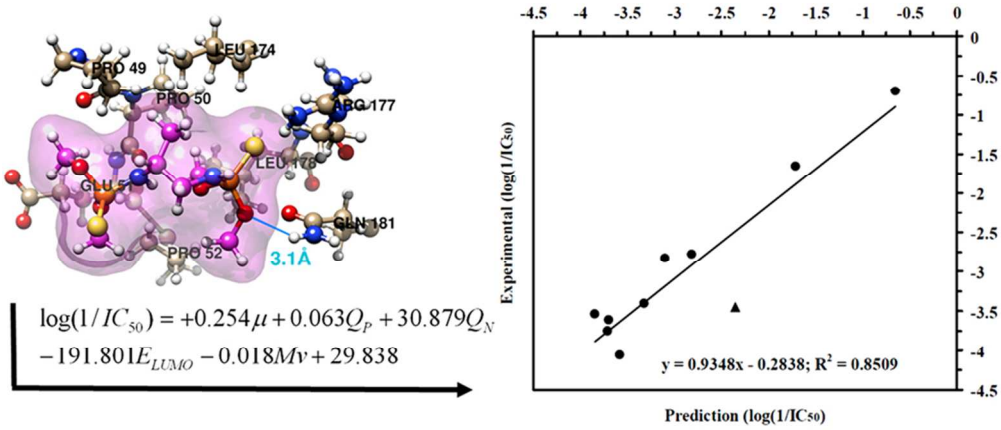

82x35mm (300 x 300 DPI)

Synthesis and crystal structure of new Temephos analogous as cholinesterase inhibitor: molecular docking, QSAR study and hydrogen bonding analysis of solid state

Khodayar Gholivand,*[a] Ali Asghar Ebrahimi Valmoozi,[a] Mahyar Bonsaii[b]

[a]Department of Chemistry, Tarbiat Modares University, P.O. Box 14115-175, Tehran, Iran

[b]Department of Chemistry, Islamic Azad University, North Tehran Branch, Tehran, Iran

ABSTRACT: A series of Temephos (Tem) derivatives were synthesized and characterized by ^{31}P, ^{13}C, ^{1}H NMR and FT–IR spectral techniques. Also, the crystal structure of compound **9** was investigated. The hydrogen bonding energies (E^2) were calculated by NBO analysis of the crystal cluster. The activities and the mixed–type mechanism of Tem derivatives were evaluated using the modified Ellman's and Lineweaver–Burk's methods on cholinesterase (ChE) enzymes. The inhibitory activities of Tem derivatives with P=S moiety were higher than those with P=O moiety. Docking analysis disclosed that the hydrogen bonds occurred between the OR (R = CH_3 and C_2H_5) oxygen and N–H nitrogen atoms of the selected compounds and the receptor site (GLN and GLU) of ChEs. PCA–QSAR indicated that the correlation coefficients of the electronic variables were dominant comparing to the structural descriptors. MLR–QSAR models clarified that the net charges of nitrogen and phosphorus atoms contribute as important electronic function in the inhibition of ChEs. Validity of QSAR model was confirmed by LOO cross–validation method with $q^2 = 0.965$ between the training and testing sets.

KEYWORDS: Bisphosphoramidothioate, Crystal structure, Cholinesterase inhibitor, QSAR, Molecular docking

■ INTRODUCTION

In recent years, organophosphorus compounds have been of great interest. A wide range of application in the areas of medicinal, agricultural, and industrial chemistry have been found owing to their significant biological and physical properties.[1] Among many known phosphorus compounds, bisphosphoramidothioates (BPAT) with the general structure of $R_1R_2P(S)NH–X–NHP(S)R_1R_2$ are important class of compounds that exhibit the insecticide properties to inhibit the cholinesterase (ChE) enzymes.[2] Little attention has been given on the interaction mechanism of the ChE enzymes and BPATs.[3,4] Temephos (Scheme 1) with the general formula is a useful insecticide to control the larvae of mosquitoes, midges and moths;[5,6] however, it has side effects on human as anti–acetylcholinesterase (AChE) and carcinogenic potential.[7] Therefore, designing and producing the selective compounds of Tem category having high insecticide potential with less anti–AChE and carcinogenic effects are required. To extend and to evaluate this problem, two new methods have so far been introduced in order to overcome the inhibition mechanism.[8] An integrated molecular docking and QSAR approaches were employed to explore the binding interactions between the Tem analogous and the AChE and butyrylcholinesterase (BChE).[9] Molecular docking was performed to define a model for the comprehension of the binding interactions between ligands and receptor. QSAR models elucidated the effective parameters of molecular structure computed by the Density Function Theory (DFT) in the inhibition process.[10] In this study, 24 novel Tem analogous with the general formula of $(RO)_2P(X)YP(X)(OR)_2$, (X = O and S; Y = NH–$(CH_2)_2$–NH, NH–$CH(CH_3)$–CH_2–NH, $N(CH_3)$–$(CH_2)_2$–$N(CH_3)$, NH–$(CH_2)_3$–NH, NH–CH_2–$C(CH_3)$–CH_2–NH, NH–$(CH_2)_4$–NH, N–$(CH_2)_4$–N, N–$(CH_2)_5$–N and NH–(C_6H_{10})–

NH; R = OCH_3 and OC_2H_5) (**1**–**24**) were synthesized and characterized by ^{31}P, ^{13}C, ^{1}H NMR and IR spectroscopy. The solid state structure of $(CH_3O)_2P(S)NH(C_6H_{10})NHP(S)(OCH_3)_2$ (**9**) was determined by X–ray crystallography and used as reference for quantum mechanical (QM) calculations at B3LYP level. The electronic aspects of two different hydrogen bonds (P=S…H–N) in the crystal structure of compound **9** were studied by NBO and Atoms in Molecules (AIM) analyses. The activities of Tem derivatives on AChE and BChE were determined using a modified Ellman's method.[11] Also the inhibition mechanisms of the prepared compounds were evaluated by Lineweaver–Burk plot.[12] Docking analysis was used to find the most efficient parameters to introduce a better mechanism of interaction between the selected molecules and the receptor site of human AChE and BChE. The appropriate molecular structural parameters were computed by DFT method and adopted to construct QSAR equations.

■ MATERIALS AND METHODS

Instrument. The enzyme AChE (human erythrocyte; Sigma, Cat. No. C0663) and BChE (bovine erythrocyte, Sigma, Cat. No. B4186), acetylthiocholine iodide (ATCh, 99%, Fluka), 5, 5'-dithiobis (2-nitrobenzoic acid)) (DTNB, 98%, Merck), Na_2HPO_4, NaH_2PO_4 (99%), ethylene diamine, propylene diamine, 1, 2-propylene diamine, 2,2-dimethylpropylene diamine, butylene diamine and 1,2-cyclohexylane diamine (99%, Merck), N,N'-dimethylethylene diamine (95%, Alfa Aesar), piperazine (99%. Acros), homopiperazine (98%, Acros), triethylamine (99.5%, Merck), $CDCl_3$ (99%, Sigma

Aldrich), $(CH_3O)_2P(S)Cl$, $(CH_3CH_2O)_2P(S)Cl$ and $(CH_3CH_2O)_2P(O)Cl$ (97%, Sigma Aldrich) were used as supplied. ^1H, ^{13}C and ^{31}P spectra were recorded on a Bruker Avance DRX 500 spectrometer. ^1H and ^{13}C chemical shifts were determined relative to internal TMS, and ^{31}P chemical shifts relative to 85% H_3PO_4 as external standard. Infrared (IR) spectra were recorded on a Shimadzu spectrometer (model IR-60) using KBr pellets. Melting points were obtained with an electrothermal instrument. UV spectrophotometer was used using a PERKIN–ELMER Lambda 25. The insecticide and anti–AChE activities of Tem derivatives were predicted by the Prediction of Activity Spectrum for Substances (PASS) software (version 1.193).[13] The three-dimensional X–ray structures of human AChE (PDB code: 1B41) and BChE (PDB code: 1POI) were chosen as the template for the modeling studies of selected compounds. The PDB files about the crystal structure of the ChE enzymes domain bound to P22303 (1B41.pdb) and P06276 (1POI.pdb) were obtained from the RCSB protein data bank (http://www.pdb.org). Molecular docking to both ChEs was carried out by using the AutoDock 4.2.3 package software.[14] The correlation analysis was performed by the Statistical Package for Social Scientists (SPSS), version 16.0 for Windows.[15] X–ray data of compound **9** were collected at 120 K on a Bruker SMART 1000 CCD area detector with graphite monochromated Mo-$K\alpha$ radiation (λ= 0.71073 Å) and refined by full-matrix least–squares methods against F^2 with *SHELXL97*.[16] CCDC 863609 contains the supplementary crystallographic data for compound **9**. These data can be obtained free of charge via http://www.ccdc.cam.ac.uk/conts/retrieving.html, or from the Cambridge Crystallographic Data Centre, 12 Union Road, Cambridge CB2 1EZ, UK; Fax: (+44) 1223-336-033; or E-mail: deposit@ccdc.cam.ac.uk.

Statistical analysis. In order to identify the effect of descriptors on the activity of AChE and BChE, QSAR studies were undertaken using the model described by Hansch and Fujita.[17] The stepwise multiple linear regression (MLR) procedure was used for model selection, which is a common method used in QSAR studies for selection descriptors. MLR fits a linear model of the form (eq 1):

$$Y = b_0 + b_1 X_1 + b_2 X_2 + ... + b_n X_k + e \qquad (1)$$

Where, Y is dependent variable, X_1, X_2, …, X_k are independent variables (descriptors), e is a random error, and b_0, b_1, b_2, …, b_k are regression coefficients.[18] The MLR method performed by the software package SPSS 16.0 was used for selection of the descriptors. The electronic and structural descriptors (X) were obtained by both the quantum chemical calculations and theoretical studies.[19] The electronic descriptors include the highest occupied and the lowest unoccupied molecular orbital (E_{HOMO} and E_{LUMO}), electrophilicity (ω), polarizability (PL) and net atomic charges (Q). Dipole moment (μ) and molecular volume (Mv) are the structural descriptors. E_{HOMO}, E_{LUMO}, ω (is expressed in terms of chemical potential and hardness), PL (the charge difference between the atoms in functional groups), Q, μ and Mv (the size and geometrical shape of the molecule and is dependent on three-dimensional coordinate of atoms in a molecule) values were obtained from the DFT results by using the Gaussian 03 program package.[20] In this study, only the variables containing the information required for modeling were used. The principal component analysis (PCA) was utilized to find the relationship between the dependent and independent variables and reducing the set of independent variables (MINITAB software, version14).[21] The linear combinations form a new set of variables,

namely principal components (PCs), which are mutually orthogonal. The first PC contains the largest variance and the second new variable contains the second largest variance and so on.[22] The validity of the QSAR model was evaluated by LOO cross-validation method, and an external data set was tested to evaluate the model. The high square value of the cross-validation coefficient (q^2) in the training set shows only a good internal validation; however, it does not automatically refer to its high validity for an external test set, because q^2 usually overestimates the validity of the model. Therefore, the QSAR model should be determined with a test set to confirm its validity. The performance of external validation was characterized by determination coefficient (R^2), standard error (S_{reg}) and q^2.[23]

Synthesis. The synthesis pathway of compounds **1-24** is represented in Scheme 2. For example, compound **1** was prepared by the reaction of a solution of diethylenamine (1 mmol) and triethylamine (2 mmol) in THF was added to a solution of $(OCH_3)_2P(S)Cl$ (2 mmol) in THF. After 4 h stirring at 0 °C, the solvent was removed in vacuum and the resulting white powder was washed with distilled solvent.

Crystal structure determination. A crystal suitable for X–ray crystallography was obtained from a mixture of THF at room temperature for compound **9** (Figure S1). The solid state structure as starting point was fully optimized by using DFT calculations in the gas phase. Whereas X–ray crystallography cannot determine accurately the position of hydrogen atoms, optimization of hydrogen atoms, positions was performed to investigate the hydrogen bond characters in solid state structures. The H atoms of N–H groups were

objectively localized in the difference Fourier synthesis and refined in isotropic approximation. To achieve this goal, the solid state structure of crystal was modeled as cluster, in which the target molecule is surrounded by two neighboring molecules (Figure 1). Other atoms were kept frozen during the optimization. Such computational justifications have also been used to describe well the geometry and electronic aspects of X-ray structure.[24,25] Taking into consideration the large number of atoms in the model cluster, all optimizations were performed at B3LYP/6–311+G** level. The NBO[26] analysis was performed to compare the electronic features of gas phase structures of compound **9** with those of the model clusters at B3LYP/6–311+G** level. Natural population analysis (NPA) was performed at the same level by using the Reed and Weinhold scheme.[27] As part of this study deals with investigation of the hydrogen bonds between S…H atoms, AIM analysis at the B3LYP/6–311+G** has much importance. Two hydrogen bonds with different lengths were observed in compound **9**. The hydrogen bonding energies were calculated on the basis of energy difference between the hydrogen bonded trimer and its fragments, as represented in equation $E_{HB} = E_{trimmer} - (E_{dimmer} + E_{monomer})$; where, dimmer is composed of two monomers (central and neighboring molecules in the right hand, in Figure 1). Then the hydrogen bonding energies were corrected for basis set superposition error (BSSE) using the counterpoise method.[24,28] All quantum chemical calculations were carried out by using the Gaussian 03 program package.[29]

Cholinesterase assay. Human cholinesterase activity measurements were performed essentially according to the method of Ellman.[11] The reaction was carried out at 37˚C in

70 mM phosphate buffer (Na_2HPO_4/NaH_2PO_4, pH=7.4) containing the AChE enzyme (10μl volume, diluted 100 times in phosphate buffer, pH=7.4), DTNB (5, 5'-dithiobis (2-nitrobenzoic acid)) (10^{-4}M concentration) and ATCh (1.35×10^{-4}M concentration). Each compound was dissolved in dimethyl sulfoxide (DMSO, 99%, Merck), which was then added to the buffer for in vitro cholinesterase assays. The highest concentration of DMSO used in the assays was 5%. In the independent experiments without the inhibitor, 5% DMSO had no effect the inhibition activity of the enzyme. The absorbance change at 37ºC was monitored with the spectrophotometer at 412 nm for 3 min, and three replicates were run in each experiment (Figure S2). In the absence of inhibitor, the absorbance change was directly proportional to the enzyme level. The reaction mixtures for determination of IC_{50} values (the median inhibitory concentration) consisted DTNB solution, 100 μl; inhibitor, x μl; acetylthiocholine iodide (ATCh) solution, 40 μl; phosphate buffer, (850–x) μl; and AChE (human erythrocyte; Sigma, Cat. No. C0663) solution, 10 μl (26.7u). The activity of BChE (bovine erythrocyte, Sigma, Cat. No. B4186) was determined the same as the AChE activity by measuring the concentration of thiocholine, which reacted with DTNB after hydrolysis of BTCh. The lyophilized BChE was diluted with 100 mM phosphate buffer (pH=7.4) for using in the activity assay. The plot of V_I/V_0 (V_I and V_0 are the activity of the enzyme in the presence and absence of inhibitors, respectively) against log[I] (where, [I] is the inhibitor's concentration) gave the IC_{50} values of 12 compounds **1**–**4**, **6**–**9**, **15**, **17**–**18**, **20** and **24** (as anti–AChE) and 11 compounds **1**–**2**, **4**, **6**–**11**, **13**, **15** and **24** (as anti–BChE) (Table 1; Figures 2A and 2B).

Inhibition mechanism study. One of the ways in which the inhibition of enzyme catalyzed reactions can be discussed, is in terms of a general scheme shown below:

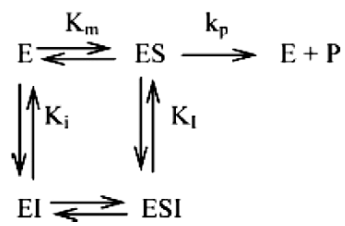

It is assumed that the enzyme-containing complexes are in equilibrium with each other, i.e. the breakdown of ES to generate product does not significantly disturb the equilibrium. In the present work, all data obtained for a particular system were analyzed using the mix model of enzyme inhibition as described in the following equation:

$$\frac{1}{V_0} = \frac{K_m(1+\frac{[I_0]}{K_i})}{V_{\max}}\frac{1}{[S_0]} + \frac{(1+\frac{[I_0]}{K_I})}{V_{\max}} \qquad (3)$$

Where, V_0 is the initial reaction rate, $V_{\max}$ is the maximum reaction rate, K_m is the Michaelis constant for the substrate to the enzyme, and K_i and K_I are the inhibition constants for binding of the inhibitor to the enzyme or to the enzyme–substrate complex, respectively. In this model, a mix inhibitor displays finite but unequal affinity for both the free enzyme (E) and the ES complex; hence, the dissociation constants from each of these enzyme forms inhibitors must be considered in their kinetic analysis.[12,30] K_i and K_I were determined using the secondary plots as described by the following equation:

$$\frac{1}{V'_{\max}} = \frac{(1+\frac{[I_0]}{K_i})}{V_{\max}} \qquad (4)$$

Slope for inhibited reaction = Slope for uninhibited reaction $\times(1+\frac{[I_0]}{K_i})$

Hence, a secondary plot of $1/V'_{max}$ against $[I_0]$ will be linear, the intercept on $[I_0]$ axis gives $-K_I$; a graph of the slope of primary plot against $[I_0]$ will also be linear, and the intercept on $[I_0]$ axis gives $-K_i$. The Lineweaver–Burk plots related to the reversible inhibitory effects of compounds showed a typical pattern of mixed inhibition (Figures 3A–3B and 3A'–3B'). The K_m and V_{max} values were calculated in the absence and presence of inhibitor from which the secondary plots were obtained, and the equilibrium dissociation constants, K_i and K_I, were calculated (Table 2). A mixed inhibitor displays affinity for both the free enzyme (K_i) and the enzyme-substrate complex (K_I). Thus, mixed–type inhibitors interfere with the substrate binding (increase K_m) and hamper the catalysis in the ES complex (decrease V_{max}). When $K_I>K_i$, the inhibitor preferentially binds to the free enzyme, and the plots cross to the left of the $1/V_0$ axis but above the $1/[S_0]$ axis (Figures 3A–3B and 3A'–3B'). In this situation, it is also termed competitive noncompetitive inhibition.

■ RESULTS AND DISCUSSION

Spectral Study. The ^{31}P NMR chemical shift at room temperature in $CDCl_3$ appears in the range 68.31–78.82 ppm for P=S and 5.42–8.64 ppm for P=O derivatives. The ^{31}P NMR spectra of compounds **2**, **9**, **11** and **18** appeared as two separated signals. The ^{1}H NMR spectrum of compound **3** revealed that two doublets at 2.76 ($^{3}J_{PNH}$ = 10.0 Hz) and 3.63 ($^{3}J_{POH}$ = 15.0 Hz) ppm are related to the methyl proton in the NCH_3 and OCH_3 groups, respectively. The ^{1}H NMR spectra of compounds **9**, **16** and **24** exhibited two signals for the methylene protons of the six membered piperazinyl rings. Two protons of

the NH group of all compounds are exhibited as a multiple peak at the range 3.48–5.37 ppm for P=S and 3.06–3.88 ppm for P=O derivatives. The ^{13}C NMR spectra of compounds **9**, **16** and **24** indicated three separated peaks for the six carbon atoms that are due to different orientations of the aliphatic six membered rings. The analysis of the IR spectra indicated that the fundamental ν(P=S) stretching modes for compounds **1**–**16** appeared at the range 770.4–955.1 cm^{-1}. The P=O stretching frequencies for compounds **17**–**24** were exhibited at the range of 1223.8–1252.1 cm^{-1}. Moreover, the N–H stretching frequencies for all compounds were observed at the range of 3189.1–3580.0 cm^{-1}.

H–bonds analysis. The crystal data and the details of the X–ray analysis of the compound **9** are given in Table S1. The phosphorus centers are in typical tetrahedral environments. The P=S bond lengths of 1.9288(9) Å and 1.9316(9) Å were observed for P(1)–S(1) and for P(2)–S(2), respectively, in $(CH_3O)_2P(S)NH(C_6H_{10})NHP(S)(OCH_3)_2$ (**9**). It seems that the difference in the bond lengths is correlated to the various orientations of cyclohexyldiamine rings and OCH_3 groups. These orientations lead to the creation of different hydrogen bonding patterns between the P=S and N–H functional groups. The one-dimensional polymeric chains form in the crystal lattice with cyclic $R_2^2(8)$ motifs in which the monomers are connected to each other *via* two P=S…H–N hydrogen bonds distance of 3.464(2) and 3.522(2) Å (Figure 1, Table 3). The $R_Y^X(Z)$ graph–set notation is descriptive of a *Z*–membered ring produced by the *X* hydrogen bonds between the *Y* donor–acceptor units.[31,32] Weak interactions, particularly P(2)–S(2)…H(3)–C(3) (2.970 Å) and P(2)–S(2)…H(2)–C(2) (2.902 Å) cause to create different hydrogen bonding lengths of the motifs. The large atomic radius and the low

electronegativity of sulfur atoms decreased the strength of the hydrogen bonding between P=S and NH. The electronic parameters of the hydrogen bonded clusters of compound **9** were calculated by AIM and NBO methods. The results of AIM and NBO analyses for the mentioned clusters are presented in Table 3 and Figure 1. As shown, the bond lengths in this cluster are equal to those obtained from the X–ray structures, except for the C–H and N–H bonds, since the optimizations have been performed only for the hydrogen atoms' positions. Also the donor–acceptor distances for the hydrogen bonds in the model cluster are equal to the experimental values. The results of AIM analysis show that the electron density (ρ) value at the bond critical point (bcp) of S(1)…H(1) (0.104 eÅ^{-3}) bond path is larger in magnitude than the that calculated for the S(2)…H(2) (0.093 eÅ^{-3}) in the model cluster. The smaller ρ value at the bcp of N–H bond confirms the presence of the stronger hydrogen bonds in P(1)–S(1)…(1)H–N(1) with the linear N–H…S contact angle in comparison with the values obtained for P(2)–S(2)…(2)H–N(2). The ρ value at the bcp of N–H bonds is 2.24 eÅ^{-3} for the fully optimized structure in the gas phase, which decreases to 2.211 and 2.217 eÅ^{-3}, respectively, in N(1)–H(1) and N(2)–H(2). The mean N–H distance increases from the isolated molecules from 1.012 Å to 1.017 Å in their hydrogen bonded of the modeled cluster. The electronic delocalization of $Lp(S)_i \rightarrow \sigma^*(N–H)_j$ occurs when the hydrogen bonds are formed between the subunits *i* and *j* within a cluster. Such an electronic effect leads to weakening of the N–H bond. It has been previously explained that the stabilizing energy E^2 increases by a decrease in the donor-acceptor distance of hydrogen bond (Gholivand and Mahzouni, 2011). The stabilizing energies E^2 of $Lp(S)_i \rightarrow \sigma^*(N–H)_j$ electron density transfer in P=S…H–N hydrogen bonds in the model cluster have been calculated as 19.94 and 16.34 kJ mol^{-1}, respectively. This

is in agreement with the values of distance for these hydrogen bonds in two P(1)–S(1)…(1)H–N(1) (3.464(2) Å) and P(2)–S(2)…(2)H–N(2) (3.522(2) Å) models. The hydrogen bonding energy in P(1)–S(1)…(1)H–N(1) model (–33.3 kJ mol^{-1}) is smaller than the value calculated for P(2)–S(2)…(2)H–N(2) (–42.4 kJ mol^{-1}), although the stabilizing energies E^2 of P=S…H–N hydrogen bonds are larger in the former (Table 3). It is noteworthy that the term E^2 refers to the stabilization energy of electronic delocalization between the donor-acceptor orbital and differs from the hydrogen bonding energy. The molecule–molecule interaction energy is the sum of the total attractive and repulsive forces between two hydrogen-bonded fragments. The results of AIM analysis revealed some critical points with very small ρ values for the C–$H_{(methyl)}$…S(2)–P(2) and C–$H_{(cyclohexane)}$…S(2)–P(2) contacts. It can be said that the steric repulsion between the diaminocyclohexane, OCH_3 group and P=S bond in the model crystal leads to a decrease in P(2)–S(2)…(2)H–N(2) hydrogen bonding energy rather than P(1)–S(1)…(1)H–N(1) model.

Prediction of biological potential. PASS software predicts 900 types of biological activities based on the structural formula.[33] The default list of predictable biological activities (P_a) includes the main and side pharmacological effects, molecular mechanisms and specific toxicities. The PASS prediction results for a compound are presented as a list of activity names and probability activity (Pa) values. The Pa values are interpreted as: if Pa > 0.7, 0.5 < Pa < 0.7, and Pa < 0.5, then the chance of finding this activity in the experiments is high, low and lower, respectively.[34,35] Insecticide potential, anti–AChE activity and carcinogenic effect of 24 newly designed molecules were obtained by using

the PASS software (Table 1). Table 1 shows that anti–AChE and carcinogenic properties of compounds decrease owing to the change of $(CH_3O)_2P{=}S$ to $(C_2H_5O)_2P{=}S$ in compounds **1**–**16**. Furthermore, the replacement of P=S in **10**–**16** to P=O in **17**–**24** increased the anti–AChE property and decreased the carcinogenic activity. The insecticidal properties of all compounds are predicted in the range of 0.496–0.635. The comparison of experimental data and the prediction of anti–AChE activities are shown in Figure S2A. As shown in Figure S2B, a linear relationship gives the plot of probable insecticide potential against anti–AChE activity. To test the anti–ChE activity of the synthesized compounds, we evaluated the inhibitory potential of titled compounds against AChE and BChE enzymes.

Bioassay. The inhibition constant (IC_{50}) values of AChE against compounds **1**–**4**, **6**–**9**, **15**, **17**–**18**, **20** were in the range of 5.01–11402.50 μM (Table 1). Compound **3** displayed the most potent inhibitory activity (IC_{50} = 5.01 μM). The inhibitory potential of compound **15** with the OC_2H_5 was more than **7** with OCH_3 substituent (Table 1). The review of literature demonstrates that the inhibitory potential of monophosphoramides (P=O moiety) is higher than the monophosphoramidothiates (P=S moiety),[36] while comparison of bisphosphoramidothioate **2** (IC_{50} = 674.53 μM) and bisphosphoramide **18** (IC_{50} = 11402.50 μM) reveals the inhibitory activity of P=S > P=O in contrast with the AChE. In the present work, the synthesized compounds **1**–**2**, **4**, **6**–**11**, **13**, **15** showed inhibition of BChE with the IC_{50} values between 149.62 and 7481.69 μM. In general, the inhibitory activities of Tem derivatives with the P=S moiety were better than the P=O moiety. The mixed–type and reversible mechanisms of these compounds were evaluated

by Lineweaver–Burk plots (Table 2). To gain a better understanding of the inhibitory potential of the synthesized compounds and to study on the reversible mechanism in more detail, it was necessary to examine the interaction of the Tem derivatives with the ChE structures by molecular docking method.

Molecular docking study. The interactions between Tem derivatives and AChE receptor were achieved by molecular docking, which can facilitate the selection of appropriate molecular parameters in the subsequent QSAR studies. The binding models of titled compounds against AChE and BChE are depicted in Figs. 2A–2D. They are located in the active site gorge of both AChE and BChE so as to maximize the favorable contacts. The hydrogen bonds and van der Waals forces are the main features of the interactions of compounds **2** (Figure 4A) and **18** (Figure 4B)with the polar charged site of AChE, as well as the interactions of **2** (Figure 4C) and **11** (Figure 4D) with the esterastic site of BChE. H–bond formation in the polar charged site was found to occur between the P–OCH_3 and P–OC_2H_5 oxygen of compounds **2** (P=S) and **18** (P=O) with the hydrogen of H–N of GLN181 (d = 3.131 Å) and GLN291 (d = 2.100 Å), respectively. Figures 4C and 4D show the 2D representation of the interaction mode of compounds **2** and **11** at the active site of BChE. It can be clearly seen from Figures 4C and 4D that the hydrogen atoms of the N–H group of compounds **2** and **11** forms an H–bond with the C=O group containing GLU197 (d = 2.760 Å) and (d = 2.822 Å) moieties. The docking data including inhibition constant (K_i), electrostatic energy (E_{elect}), and the rest of H–bonds distance are given for the ChEs in Table S3. Figs. 3A and 3A' indicate that the increase of the H–bond distances of RO…H–N leads to enhance their inhibitory potential, while

these correlations are reversed in the interaction between BChE and ligands (Figures 5B and 5B'). To continue work, QSAR technique was used to find the effective electronic and structural parameters.

QSAR analysis. QSAR studies were done in order to recognize the effect of descriptors on the activity of AChE and BChE enzymes. The stepwise MLR procedure, which is a common method used in QSAR studies was used for model selection. The electronic and structural descriptors were obtained by quantum chemical calculations (Table S3). The number of independent variables is equal to the training set compounds, as shown in Tables 1 and S3. Therefore, PCA method was used to reduce the independent variables. The variable selection in PCA was performed by using the Fisher's weights approach[37] and the results are summarized as the following equations (4a and 4b):

$$PC_1 = +0.411Q_{P(1)} + 0.411Q_{P(2)} - 0.400Q_{X(S,O)} - 0.080Q_N + 0.410PL_{P=X} - 0.407E_{HOMO} - 0.052E_{LUMO} + 0.316\omega + 0.142\mu + 0.035Mv \quad (4a)$$

$$PC_2 = +0.064Q_{P(1)} + 0.053Q_{P(2)} - 0.042Q_{X(S,O)} + 0.547Q_N + 0.121PL_{P=X} - 0.028E_{HOMO} + 0.500E_{LUMO} - 0.334\omega + 0.343\mu + 0.437Mv \quad (4b)$$

The results showed the total variance of the first and second factor PC was 51.4% and 19.0%, respectively. Figure S3 shows the score and the loading plot of $PC_1 \times PC_2$. The score plot shows that separation of the compounds with P=O (right side) and P=S (left side) groups has been provided by PC_1, which contains the most part of the variance. From the above equations, it is deduced that the electronic parameters (Q_P, Q_X, Q_N, $PL_{P=X}$, E_{LUMO}, E_{HOMO} and ω) are the largest comparing to the structural parameters (μ and Mv). Consequently, these nine descriptors with higher correlation coefficient were

selected to carry out the stepwise multiple linear regression (MLR) analysis, which led to an optimal QSAR equation based on the anti–AChE potency (eq 5):

$$\begin{aligned}\log(1/IC_{50}) &= +0.017\mu + 64.805Q_P + 1.690Q_{X(S,O)} - 8.967Q_N - 31.967PL_{P=X} \\ &- 25.193E_{HOMO} - 217.942E_{LUMO} - 243.834\omega + 0.016Mv - 33.690 \\ n &= 13; R^2 = 0.721; S_{reg} = 0.966; F_{\text{statistic}} = 0.862\end{aligned} \quad (5)$$

Where, n is the number of compounds, R^2 is the determination coefficient of regression, S_{reg} is the standard deviation of regression and $F_{\text{statistic}}$ is the Fisher's statistic.[38] The variables with a high value of Variance Inflation Factor (VIF >10) are candidates for exclusion from the model.[39] The low determination coefficient value (R^2 = 0.721) and high residual value (S_{reg} = 0.966) with high VIF value (see Table 4) are associated with the multicollinearity problem. The improvement in eq 3 was carried out by omitting of compounds **7**, **8**, **24** from the training set compounds and replacing E_{LUMO} with ω and E_{HOMO}, as well as Q_{P} with $PL_{\text{P=X}}$ and Q_{X}. The linear regression was performed using the remaining five parameters that yielded the following model with increasing of R^2 = 0.922 and decreasing of S_{reg} = 0.438 (eq 6):

$$\begin{aligned}\log(1/\text{IC}_{50}) &= +0.175\mu + 0.845Q_P + 29.699Q_N - 129.903E_{LUMO} - 0.019Mv + 27.921 \\ n &= 10; R^2 = 0.922; S_{reg} = 0.438; F_{\text{statistic}} = 9.473\end{aligned} \quad (6)$$

The correlating parameters have VIF<10; thus, there is no colinearity problem (Table 4). In this equation, the inhibitory potency of AChE is influenced mainly by the electronic parameters. E_{LUMO} with the coefficient value of –129.903 has the highest contribution to $\log(1/IC_{50})$ rather than the structural parameters. The negative sings of E_{LUMO} in $\log(1/IC_{50})$ disclose that the compound with lower E_{LUMO} is indicative of higher toxicity against the AChE enzyme. The net charge of N–H nitrogen (Q_{N}) with the coefficient

value of +29.699 reveals the highest effect of function on the inhibitory potential rather than the net charge of P=O phosphorus (+0.845). The correlation matrix was used to determine the interrelationship between the independent variables. A high interrelationship was observed between E_{LUMO} and Q_{N} (r = +0.456) (Table 5). Therefore, compound **3** with Q_{N} = –0.893 and compound **18** with Q_{N} = –1.031 showed the highest and the lowest inhibitory potential, respectively. Consequently, the net charge of nitrogen atom is able to control the influence of molecular orbital energy in inhibition of human AChE. Also the interaction of BChE as a secondary target was investigated against the tested compounds (**1**–**24**) and the same procedures were carried out. The QSAR modification model based on anti–BChE potency produced the following equation:

$$\begin{aligned}&\log(1/IC_{50}) = -0.148\mu + 7.065Q_P + 1.720Q_{X(S,O)} + 0.430Q_N + 0.469PL_{P=X}\\&+100.702E_{HOMO} - 100.525E_{LUMO} - 104.965\omega - 0.002Mv + 22.751\\&n = 12; R^2 = 0.566; S_{reg} = 0.862; F_{\text{statistic}} = 0.290\end{aligned} \tag{7}$$

Table 4 shows that the regression equation is not favorable with VIF>10. The improvement in eq 7 was performed by excluding compounds **1**, **24** from the selected compounds and replacing ω with E_{LUMO} and E_{HOMO}, as well as Q_{P} with $PL_{\mathrm{P=X}}$ and Q_{X}. Consequently, a new multiple regression was resulted without colinearity (eq 8):

$$\begin{aligned}&\log(1/IC_{50}) = -0.116\mu + 3.768Q_P - 0.32Q_N - 106.212\omega + 0.004Mv + 3.397\\&n = 10; R^2 = 0.848; S_{reg} = 0.352; F_{\text{statistic}} = 4.479\end{aligned} \tag{8}$$

The model described by eq 8, similar to eq 6, depicts the share of molecular orbital energy in the inhibition of BChE. The most effective variable in the interaction of BChE and Tem derivatives was ω with the coefficient value of –106.212. The interrelationship between the variables and the correlation matrix results are presented in Table 5. The high interrelationship between ω and Q_{P} (r = +0.680) shows that Q_{P} controls the affect of

molecular orbital energy in the inhibition of human BChE. Compounds **15** (Q_P = +2.027) and **2** (Q_P = +1.997) are in order of the highest and the lowest inhibitory potential. DFT–QSAR models of AChE and BChE revealed that changing in the net charge of nitrogen and phosphorus atoms contributes an important function in the inhibition mechanism of AChE and BChE, respectively. The above results are relatively good, but the validity of QSAR models and docking output must be examined by NBO and LOO cross validation methods.

Validation of MLR-QSAR Model. The LOO cross–validation method was used for the training sets to select the optimum values of parameters. This procedure consists three stage; i) removing one sample from the training set, ii) constructing the equation on the basis of only the remaining training data, and iii) testing of the model on the removed and innovative samples.[40] The total of 10 samples were used as a training set, and the remaining compounds (**7**, **8** and **24)** for AChE–QSAR (eq 6) were adopted as a test set for validating the models. A new equation is proposed to determine the outliers using LOO cross–validation coefficient q^2_{n-i}, which is equal to the q^2 of compound *i* computed by the new cross-validation procedure after leaving this datum from *n* compounds. The compound with unduly high q^2_{n-i} value can be considered as an outlier, and the compound with low value can be taken as an influential point. Compound **4** has too large q^2_{n-i} value in the training set, so this compound can be confirmed to be an outlier from the AChE–QSAR model. After omitting compound **4**, two optimal models are obtained (eq 9):

$$\log(1/IC_{50}) = +0.254\mu + 0.063Q_P + 30.879Q_N - 191.801E_{LUMO} - 0.018Mv + 29.838$$

$$n = 9; R^2_{Adj} = 0.907; S_{reg} = 0.335; r = 0.10; \quad (9)$$
$$F_{\text{statistic}} = 16.59; q^2 = 0.965; P < 0.0214$$

Where, q^2 is the square of LOO cross–validation coefficient. A good QSAR model has characters of large *F*, small *r* and S_{reg}, low *P*–value, and R^2 and q^2 values close to 1.[41] So the above established eq 9 shows appropriate statistical quality. To check the validity of eq 9, we selected our previous omitted compound (**4**) as the test set; the dependent and independent variables with their residuals of test set compounds are shown in Table 1. Table 1 and particularly residuals data show that the inhibition results are the same in the empirical and prediction techniques. Figure 6 indicates that the predicted values of $\log(1/IC_{50})$ are in good agreement with the experimental ones. The integrity was validated by the determination coefficient of R^2 = 0.851 with the residuals between the training and testing sets.

Natural Bond Orbital (NBO) analysis. The stabilization energies (E^2) data clarify that electron transfers lead to change in the net charge of phosphorus and nitrogen atoms, and accordingly, alter the inhibitory properties of compounds against enzymes. The NBO analysis reveals an electronic delocalization between the lone pair of X atom in the P=X(O, S) group, Lp(X_P), and the vacant $\sigma^*(P-O_2)$ orbital. Stabilization energies of 9.211 kJ/mol for compound **2** with the P=S moiety, and 103.706 kJ/mol for compound **18** with the P=O moiety were obtained for the $Lp(X_P) \rightarrow \sigma^*(P-O_2)$ interaction (Table 6). The this interaction increases the electron density of OR (R = CH_3 and C_2H_5) oxygen

atom and rises the hydrogen bond energy of $(R–O)_{ligand}…(H–N)_{enzyme}$ type (Figure 4). Comparing to **18**, compound **2** has higher inhibitory potential in contrast to AChE. The H–bond energy of CH_3–O…H–N (GLN181) for compound **2** is lower than the energy of C_2H_5–O…H–N (GLN291) for compound **18**. Hence, there is not a direct correlation between the E^2 of $Lp(X_P) \rightarrow \sigma^*(P-O_2)$ interaction and the hydrogen bond energy against the AChE activity. In other words, compound **2** with E^2 = 18.601 kJ/mol and compound **18** with E^2 = 16.218 kJ/mol for the $Lp(X_P) \rightarrow \sigma^*(P-N_1)$ interaction (Table 6) prove that the negative charge of nitrogen atom (Q_N) versus the hydrogen bond energy of $(R–O)_{ligand}…(H–N)_{protein}$ affects on the log(1/IC_{50}) factor. For instance, compound **3** with the highest E^2 and Q_N behaves as a strong inhibitor in the process of the inhibition of AChE. In addition, the high E^2 = 16.678 kJ/mol of $Lp(N_1) \rightarrow \sigma^*(P-O_2)$ interaction for compound **18** comparing to compound **2** (E^2 = 12.582 kJ/mol) leads to the increase of the electron density of oxygen atom on the alcohol substituent and consequently to the rise of the energy of the hydrogen bonding and to the decline of the inhibition potential. By investigating the interaction mechanism of ligand and BChE enzyme, it can be said that the $Lp(O_2) \rightarrow \sigma^*(P-N_1)$ interaction of selected compounds (**2** and **11**) increases the electron density of N–H nitrogen and rises of the hydrogen bond energy of $(N–H)_{ligand}…(O=C)_{enzyme}$ type (Figure 4). The H–bond energy of N–H…O=C (GLU197) for compound **2** is higher than that of **11,** while compound **2** has lower inhibitory potential comparing to compound **11** in contrast to BChE. It means that the net charge of phosphorus atom's (Q_P) effect inverses the H–bond energy of $(N–H)_{ligand}…(O=C)_{enzyme}$. Figures 5A" and 5B" demonstrate that the H–bonds energy of the docking analysis of AChE and BChE has negative proportional to the Q_N and Q_P parameters.

■ CONCLUDING REMARKS

Twenty four bisphosphoramidothioate with the general formula of $(RO)_2P(S)XP(S)(OR)_2$ (**1**–**24**) were synthesized and characterized by spectroscopy methods. The cyclic motif of $(CH_3O)_2P(S)NH(C_6H_{10})NHP(S)(OCH_3)_2$ (**9**) was determined by X–ray crystallography. The results of NBO analysis showed that the H–bond energy in P(1)–S(1)…(1)H–N(1) and P(2)–S(2)…(2)H–N(2) model was –33.3 and –42.4 kJ mol^{-1}, respectively. Docking analysis disclosed the reversible noncovalent interactions, especially hydrogen bonds occurred between the OR (R = CH_3 and C_2H_5) oxygen and N–H nitrogen atoms of selected compounds, and the H–N atoms of GLN with O=C of GLU. The MLR–QSAR models (to R^2=0.922 and 3.422 < VIF < 12.411 for AChE and to R^2=0.845 and 1.281 < VIF < 3.105 for BChE) and correlation matrix clarified that the net charge of N–H nitrogen and R_2NP=X phosphorus atoms contribute as important electronic function in the inhibition of ChEs. The interrelationship shows that the net charge of nitrogen and phosphorus atoms control the modification of the molecular orbital energy of Tem analogues. The predicted values of $\log(1/IC_{50})$ are in good agreement with the experimental ones; the validity of QSAR model was confirmed by LOO cross–validation method with $q^2 = 0.965$ between the training and testing sets. Increasing of E^2 for the $Lp(X_P) \rightarrow \sigma^*(P-N)$ and $Lp(N) \rightarrow \sigma^*(P-O)$ interactions and the electron density of the N–H nitrogen with the OR oxygen of Tem analogous verifies the integrity of QSAR equation and docking results in the inhibition process of ChE enzymes.

■ AUTHOR INFORMATION

Corresponding Author

*Phone: +98 21 82883443; fax: +98 218006544; e-mail gholi_kh@modares.ac.ir

■ SUPPORTING INFORMATION

Spectral data as indicated in the text relative to Tem analogous (**1**–**24**). This information is available free of charge via the Internet at http: //pubs.acs.org.

■ ABBREVIATIONS USED

AChE, Acetylcholinesterase; BPAT, Bisphosphoramidothioate; ChE, Cholinesterase; DFT, Density function theory; IC_{50}, Half maximal inhibitory concentration; PASS, Prediction of activity spectrum for substances; PCA, principal component analysis; PDB, Protein data bonk; QSAR, Quantitative structure–activity relationships; SPSS, Statistical package for social scientists; Tem, Temephos; VIF, Variance inflation factor;

■ REFRENCES

(1) Olszewski, T. K.; ˛zowska, J. G.; Boduszek, B.; Kozłowski, H. New Heterocyclic Mono- and Bis(α-hydroxymethyl)phosphinic Acids: Synthesis and CuII Binding Abilities. *Eur. J. Org. Chem.* **2007**, 3539–3546.

(2) Dos Santos, V. M. R.; Sant Anna, C. M. R.; Borja, G. E. M.; Chaaban, A.; Cortes, W. S.; Da Costa, J. B. N. New bisphosphorothioates and bisphosphoroamidates: Synthesis, molecular modeling and determination of insecticide and toxicological profile. *Bioorg. Chem.* **2007**, 35, 68–81.

(3) Kaboudin, B.; Emadi S.; Hadizadeh, A. Synthesis of novel phosphorothioates and phosphorodithioates and their differential inhibition of cholinesterases. *Bioorg. Chem.* **2009**, 37, 101–105

(4) Fest, C.; Schmidt, K. J. The Chemistry of Organophosphorus Pesticides, Springer-Verlag, Berlin–Heidelberg–New York, 1982.

(5) Lores, E. M.; Moore, J. C.; Moody, P.; Clark, J.; Forester, J.; Knight, J. Temephose residues in stagnant pond after mosquito larvicide application by helicopter. *Bull. Environ. Contam. Toxicol.* **1985**, 35, 308–313.

(6) Tikar, S. N.; Kumar, A.; Prasad, G. B. K. S.; Prakash, S. Temephos-induced resistance in Aedes aegypti and its cross-resistance studies to certain insecticides from India. *Parasitol. Res*. **2009**, 105, 57–63.

(7) Hackenberger, B. K.; Perkusic, D. J.; Stepic, S. Effect of temephos on cholinesterase activity in the earthworm *Eisenia fetida* (Oligochaeta, Lumbricidae). *Ecotoxic. Environ. Saf.* **2008**, 71, 583–589.

(8) Ba-Omar, T. A.; Al-Jardani, S.; Victor, R. Effects of pesticide temephos on the gills of Aphanius dispar (Pisces: Cyprinodontidae). *Tiss. Cel*. **2011**, 43, 29–38.

(9) Amadasi, A.; Mozzarelli, A.; Meda, C.; Maggi, A.; Cozzini, P. Identification of xenoestrogens in food additives by an integrated in silico and in vitro approach. *Chem. Res. Toxicol.* **2009**, 22, 52–63.

(10) Modesto, C.; Luciana, S.; Antonio, C.; Cosimo, A.; Adele, N.; Saverio, C.; Angelo, C. Investigation of platelet aggregation inhibitory activity by phenyl amides and esters of piperidinecarboxylic acids. *Bioorg. Med. Chem.* **2003**, 11, 439–1450.

(11) Ellman, G. L.; Coutney, K. D.; Andres, V. R.; Featherstone, M. A new and rapid colorimetric determination of acetylcholinesterase activity. *Biochem. Pharmacol*. **1961**, 7, 91–95.

(12) Copeland, R. A. Enzymes, A Practical Introduction to Structure, Mechanism, and Data Analysis, Second ed. John Wiley-VCH, New York, 2000.

(13) Lagunin, A.; Stepanchikova A.; Filimonov D.; Poroikov, V. PASS: Prediction of activity spectra for biologically active substances. *Bioinformatics Applications Note*. **2000**, 16, 747–748.

(14) Morris, G. M.; Goodsell, D. S.; Halliday, R. S.; Huey, R.; Hart, W. E.; Belew, R. K.; Olson, A. J. J. Comput. Chem. **1998**, 19, 1639–1662.

(15) SPSS for Windows, Version 10.05, SPSS Inc., Bangalore, India, 1999.

(16) Sheldrick, G. M. A short history of *SHELX*. *Acta. Cryst.* **2008**, A64, 112–122.

(17) Hansch, C.; Fujita, T. *p*-σ-π Analysis. A method for the correlation of biological activity and chemical structure. *J. Am. Chem. Soc.* **1964**, 86, 1616–1626.

(18) Jung, M.; Tak, J.; Lee, Y.; Jung, Y. Quantitative structure–activity relationship (QSAR) of tacrine derivatives against acetylcholinesterase (AChE) activity using variable selections. *Bioorg. Med. Chem. Letters.* **2007**, 17, 1082–1090.

(19) De melo, E. B. Multivariate SAR/QSAR of 3-aryl-4-hydroxyquinolin-2(1H)-one derivatives as type I fatty acid synthase (FAS) inhibitors. *Europ. J. Med. Chem.* **2010**, 45, 5817–5826.

(20) Sharma, S. K.; Kumar, P.; Narasimhan, B.; Ramasamy, K.; Mani, V.; Mishra, R. K.; Majeed, A. A. Synthesis, antimicrobial, anticancer evaluation and QSAR studies of 6-methyl-4-[1-(2-substituted-phenylamino-acetyl)-1H-indol-3-yl]-2-oxo/thioxo-1,2,3,4-tetrahydropyrimidine-5-carboxylic acid ethyl esters. *Eur. J. Med. Chem*. **2012**, 48, 16–25.

(21) Pinto, M. F. S.; Romero, O. A. S.; Pinheiro, J. C. Pattern recognition study of structure–activity relationship of halophenols and halonitrophenols against fungus T. mentagrophytes. *J. Mol. Struct. (Theochem).* **2001**, 539, 303–310.

(22) Malta, V. R. S.; Pinto, A. V.; Molfetta, F. A.; Honório, K. M.; de Simone, C. A.; Pereira, M. A.; Santos, R. H. A.; da Silva, A. B. F. The influence of electronic and steric effects in the structure–activity relationship (SAR) study of quinone compounds with biological activity against Trypanosoma cruzi. *J. Mol. Struct. (Theochem)*. **2003**, 634, 271–280.

(23) Schuurmann, G.; Ebert, R. U.; Chen, J. W.; Wang, B.; Kuhne, R. External Validation and Prediction Employing the Predictive Squared Correlation Coefficient — Test Set Activity Mean vs Training Set Activity Mean. *J. Chem. Inf. Model.* **2008**, 48, 2140–2145.

(24) Mirzaei, M.; Elmi, F.; Hadipour, N. L. A Systematic Investigation of Hydrogen-Bonding Effects on the ^{17}O, ^{14}N, and ^{2}H Nuclear Quadrupole Resonance Parameters of Anhydrous and Monohydrated

Cytosine Crystalline Structures: A Density Functional Theory Study. *J. Phys. Chem. B.* **2006**, 110, 10991–10996.

(25) Gholivand K.; Ebrahimi Valmoozi A. A.; Mahzouni H. R. Structural and electronic aspects of hydrogen bonding in two polymorphs of butylene-N,N_-bis(O,O_-diarylphosphoramidate). *Acta. Cryst.* **2013**, B69, 55–61.

(26) Reed, A. E.; Curtiss, L. A.; Weinhold, F. Intermolecular interactions from a natural bond orbital, donor–acceptor viewpoint. *Chem. Rev.* **1988**, 88, 899–926.

(27) Carpenter, J. E.; Weinhold, F. Analysis of the geometry of the hydroxymethyl radical by the "different hybrids for different spins" natural bond orbital procedure. *J. Mol. Struct. (Theochem).* **1988**, 169, 41–46.

(28) Boys, S. F.; Bernardi, F. The calculation of small molecular interactions by the differences of separate total energies. Some procedures with reduced errors. *Mol. Phys.* **1970**, 19, 553–566.

(29) Frisch, M. J.; Trucks, G. W.; Schlegel, H. B.; Scuseria, G. E.; Robb, M. A.; Cheeseman, J. R.; Montgomery J. A.; Vreven, T.; Kudin, K. N.; Burant, J. C.; Millam, J. M.; Iyengar, S. S.; Tomasi, J.; Barone, V.; Mennucci, B.; Cossi, M.; Scalmani, G.; Rega, N.; Petersson, G.A.; Nakatsuji, H.; Hada, M.; Ehara, M.; Toyota, K.; Fukuda, R.; Hasegawa, J.; Ishida, M.; Nakajima, T.; Honda, Y.; Kitao, O.; Nakai, H.; Klene, M.; Li, X.; Knox, J. E.; Hratchian, H. P.; Cross, J. B.; Bakken, V.; Adamo, C.; Jaramillo, J.; Gomperts, R.; Stratmann, R. E.; Yazyev, O.; Austin, A. J.; Cammi, R.; Pomelli, C.; Ochterski, J. W.; Ayala, P. Y.; Morokuma, K.; Voth, G. A.; Salvador, P.; Dannenberg, J. J.; Zakrzewski, V. G.; Dapprich, S.; Daniels, A. D.; Strain, M. C.; Farkas, O.; Malick, D. K.; Rabuck, A. D.; Raghavachari, K.; Foresman, J. B.; Ortiz, J. V.; Cui, Q.; Baboul, A. G.; Clifford, S.; Cioslowski, J.; Stefanov, B. B.; Liu, G.; Liashenko, A.; Piskorz, P.; Komaromi, I.; Martin, R. L.; Fox, D. J.; Keith, T.; Al-Laham, M. A.; Peng, C. Y.; Nanayakkara, A.; Challacombe, M.; Gill, P. M. W.; Johnson, B.; Chen, W.; Wong, M. W.; Gonzalez, C.; Pople, J. A. Gaussian 03, Revision D.01, Gaussian, Inc., Wallingford CT, 2005.

(30) Dabirmanesh, B.; Khajeh, K.; Ranjbar, B.; Ghazi, F.; Heydari, A. Heydari, Inhibition mediated stabilization effect of imidazolium based ionic liquids on alcohol dehydrogenase. *J. Mol. Liq.* **2012**, 170, 66–71.

(31) Bernstein, J.; Davis, R. E.; Shimoni, L.; Chang, N. L. Patterns in hydrogen bonding: Functionality and graph set analysis in crystals. *Angew. Chem. Int. Ed.* **1995**, 34, 1555–1573.

(32) Gholivand, K.; Mahzouni, H. R. Solid-state and gas-phase structures of two conformers of N-(4-methylphenyl)-N′,N"-bis(morpholinyl) phosphoric triamide; insights from X-ray crystallography and DFT calculations. *Acta. Cryst.* **2011**, B67, 238–243.

(33) *PASS*., Software. Version 1.917-July, 2005.

(34) Geronikaki, A. A.; Dearden, J. C.; Filimonov, D.; Galaeva, I.; Garibova, L.; Gloriozova, T.; Kranjneva, V.; Lagunin, A.; Macaev, F. Z.; Molodavkin, G.; Poroikov, V.; Pobrebnoi, S. I.; Shepeli, F.; Voronina, T.; Tsitlakido, M.; Vald, L. Design of new cognition enhancers: from computer prediction to synthesis and biological evaluation. *J. Med. Chem.* **2004**, 47, 2870–2876.

(35) Lagunin, A.; Stepanchikova, A.; Filimonov, D.; Poroikov V. PASS. *Bioinf. appl. note.* **2000**, 16, 747–748.

(36) Ghadimi, S.; Asad-Samani, K.; Ebrahimi-Valmoozi, A. A. Synthesis, Spectroscopic Characterization and Structure-Activity Relationship of Some Phosphoramidothioate Pesticides. *J. Iran. Chem. Soc.* **2011**, 8, 717–726.

(37) Soltani, S.; Abolhasani, H.; Zarghi, A.; Jouyban, A. A. QSAR analysis of diaryl COX–2 inhibitors: comparison of feature selection and train-test data selection methods. *Eur. J. Med. Chem*. **2010**, 45, 2753–2760.

(38) Roy, D. R.; Sarkar, U.; Chattaraj, P. K.; Mitra, A.; Padmanabhan, J.; Parthasarathi, R.; Subramanian, V.; Van Damme, S.; Bultinck, P. Analyzing toxicity through electrophilicity. *Mol. Divers.* **2006**, 10, 119–131.

(39) Singh, J.; Shaik1, B.; Singh, S.; Agrawal, V. K.; Khadikar, P. V.; Deeb, O.; Supuran, C. T. Comparative QSAR Study on Para-substituted Aromatic Sulphonamides as CAII Inhibitors: Information versus Topological (Distance–Based and Connectivity) Indices. *Chem. Biol. Drug. Des.* **2008**, 71, 244–259.

(40) Hua, R.; Doucet, J. P.; Delamar, M.; Zhang, R. QSAR models for 2-amino-6-arylsulfonylbenzonitriles and congeners HIV-1 reverse transcriptase inhibitors based on linear and nonlinear regression methods. *Eur. J. Med. Chem.* **2009**, 44, 2158–2171.

(41) Liao, S. Y.; Chen, J. C.; Qian, L.; Shen, Y.; Zheng, K. C. QSAR, action mechanism and molecular design of flavone and isoflavone derivatives with cytotoxicity against HeLa. *Eur. J. Med. Chem.* **2008**, 43, 2159–2170.

Figure Captions

Figure 1. Illustration of $R_2^2(8)$ graph sets in $(CH_3O)_2P(S)NH(C_6H_{10})NHP(O)(OCH_3)_2$; a model to describe the hydrogen-bonded cluster for DFT calculations, in which molecule is the target molecule in the center. A similar model was considered for another molecule, in which molecule in the center is the target molecule.

Figure 2. The plot of V_I/V_0 against log[I] for inhibitors. V_I and V_0 are the AChE (A) and BChE (B) enzyme's activities (OD min^{-1}), and [I] is the inhibitor concentration (μM).

Figure 3. (A and B) The plot of 1/[V] against 1/[S] for the inhibitors **1** and **2** against BChE and AChE activation without inhibitor. [V] is the enzyme activity (OD min^{-1}) and [S] is the ATCh concentration (mM). (A' and B') Steady state inhibition of AChE by compounds **1** and **2**. Secondary replots of the Lineweaver–Burk plot: $1/V_{maxapp}$ or slope versus various concentrations of the inhibitor.

Figure 4. (A, B) 2D model of H–bond formation in the polar charged site, between the P–OCH_3 and P–OC_2H_5 oxygen **2** (A) and **18** (B) and the hydrogen of H–N of GLN181 (d = 3.131 Å) and GLN291 (d = 2.100 Å) of AChE enzyme. (C, D) 2D model of the hydrogen atoms of the N–H group of compounds **2** (C) and **11** (D) forms an H–bond with the C=O group containing GLU197 (d = 2.760 Å) and (d = 2.822 Å) of BChE enzyme.

Figure 5. The linear plot of the electrostatic energy of docking analysis against log($1/IC_{50}$) for AChE (A) and for BChE (B). The linear plot of the H-bond energy against the electrostatic energy of docking analysis for AChE (A') and for BChE (B'). The linear plot of the H–bond energy of docking analysis against E_{LUMO} for AChE (A"), and against ω for BChE (B").

Figure 6. Plot of predicted activities versus experimental ones for the QSAR model, in which 10 compounds are the training set (●) and correspondingly one compound is the test set (▲).

Scheme 1. Synthesis pathway and chemical structure of compounds **1-24**.

Table 1. Experimental, predication and external validation step of the biological activity of the BPAT compounds

No.	Prediction (PASS)			Experimental				External validation	
				IC_{50}		$log(1/IC_{50})_{Expt.}$		$log(1/IC_{50})_{Pred.}$[a]	
	anti-AChE	Carcinogenic	Insecticide	AChE	BChE	AChE	BChE	AChE	Res.[b]
1	0.474	0.537	0.607	2546.83	273.53	-3.406	-2.437	-3.323	0.083
2	0.421	0.493	0.567	674.53	6338.70	-2.829	-3.802	-3.102	0.273
3	0.702	0.813	0.610	5.01	----	-0.700	----	-0.655	0.045
4	0.589	0.451	0.566	2805.43	7481.69	-3.448	-3.874	-2.357	1.091
5	0.420	0.477	0.582	----	----	----	----	----	----
6	0.586	0.478	0.572	5636.37	175.39	-3.751	-2.244	-3.712	0.039
7	0.571	0.631	0.635	912.01	164.81	-2.960	-2.244	-0.616	2.344
8	0.466	0.514	0.561	1119.44	874.98	-3.049	-2.942	-0.645	2.404
9	0.527	0.547	0.580	602.56	891.25	-2.780	-2.950	-2.818	0.038
10	0.435	0.221	0.582	----	717.80	----	-2.855	----	----
11	0.409	0.228	0.556	----	520.00	----	-2.716	----	----
12	0.632	0.565	0.582	----	----	----	----	----	----
13	0.553	0.000	0.546	----	346.73	----	-2.540	----	----
14	0.409	0.206	0.571	----	----	----	----	----	----
15	0.483	0.466	0.579	44.98	149.62	-1.653	-2.175	-1.715	0.062
16	0.491	0.249	0.558	----	----	----	----	----	----
17	0.592	0.224	0.569	4055.08	----	-3.608	----	-3.701	0.093
18	0.540	0.000	0.524	11402.50	----	-4.057	----	-3.584	0.473
19	0.821	0.366	0.527	----	----	----	----	----	----
20	0.680	0.000	0.532	3467.37	----	-3.540	----	-3.846	0.306
21	0.565	0.000	0.558	----	----	----	----	----	----
22	0.677	0.000	0.539	----	----	----	----	----	----
23	0.442	0.807	0.496	----	----	----	----	----	----
24	0.569	0.232	0.507	363.08	851.14	-2.560	-2.930	-3.683	1.123

[a] Predictive activities were calculated using the QSAR model.
[b] Residual for molecule is the difference between the experimental and predicted property.

Table 2. Experimental parameters of the AChE and BChE activities of titled compounds

Enzyme	No.	K_m (mM)	K_i[a] (mM)	K_I[b] (mM)	V_m (mM/min)	Inhibition Mechanism
BChE	**1**	0.107	1.537	5.338	1.696	MT[a]
	2	0.133	0.362	2.286	2.108	MT
	3	0.084	1.925	1.137	2.716	MT
AChE	**4**	0.095	2.913	1.515	2.038	MT
	7	0.080	0.121	0.377	2.194	MT
	8	0.075	0.317	1.541	1.996	MT

[a] MT = Mixed type;
[b] K_i = Inhibitor affinity for the free enzyme;
[c] K_I = Inhibitor affinity for enzyme-substrate complex.

Table 3. Hydrogen bonds data for the X-ray structure (the values in brackets), model cluster (at B3LYP/6-311+G), charge densities (from AIM analysis), delocalization energy (from NBO analysis) and bonding energy (at B3LYP/6-311+G**) for the model cluster.**

D-H. . .A	*d*(N–H)	*d*(H. . .S)	*d*(N. . .S)	∠NHS	*ρ* at the b.c.p. (eÅ^{-3})		$E^{(2)a}$	$E_{HB}{}^{b}$
					N–H	H...S		
N(1)–H(1N)...S(1)[c]	[1.016]0.850	[2.50]2.70	[3.464(2)]	[157.1]151.0	0.328	0.104	19.94	–33.3
N(2)–H(2N)...S(2)[d]	[1.017]0.880	[2.55]2.71	[3.522(2)]	[155.7]154.0	0.329	0.093	16.34	–42.4

[a] The stabilizing energy E^2 refers to the effect of $Lp(X_P)_i \rightarrow \sigma^*(N–H)_j$ delocalization. [b] The binding energy in kJ mol^{-1} for N–H...S hydrogen bonds. [c] –x+2, –y+1, –z; [d] –x+2, –y, –z+1.

Table 4. VIF[a] values for the QSAR equations

Independent variable	AChE		BChE	
	eq 2	eq 3	eq 4	eq 5
Q_P	5154.635	4.060	2416.392	2.122
$Q_{X(S,O)}$	82.623		70.221	
Q_N	46.154	12.411	31.865	3.105
$PL_{P=X}$	6368.558		3547.065	
E_{HOMO}	1677.977		313.179	
E_{LUMO}	1529.029	3.422	468.766	
ω	3249.905		688.616	2.629
μ	7.195	4.140	26.590	1.281
Mv	6.540	6.665	10.261	2.635

[a] VIF = $1/(1-R_i^2)$; where, R_i is the multiple correlation coefficient of the *i*th independent variable on all of the other independent variables.

Table 5. Correlation matrix for the anti–AChE and anti–BChE parameters and the selected variables in eq 6 and eq 8.

Selected variables	AChE					Selected variables	BChE				
	μ	Q_P	Q_N	E_{LUMO}	Mv		μ	Q_P	Q_N	ω	Mv
μ	1.000					μ	1.000				
Q_P	+0.307	1.000				Q_P	+0.062	1.000			
Q_N	–0.520	–0.427	1.000			Q_N	+0.304	–0.204	1.000		
E_{LUMO}	+0.101	–0.209	+0.459	1.000		ω	–0.268	+0.680	–0.407	1.000	
Mv	+0.105	+0.417	+0.404	–0.033	1.000	Mv	+0.246	+0.077	+0.734	–0.049	1.000

Table 6. Stabilization energies (E^2) of the NBO analysis some of compounds

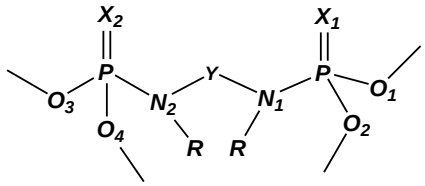

Electronic delocalization	E^2 (kJ/mol)			
	2	**3**	**11**	**18**
$Lp(X_1) \rightarrow \sigma^*(P-N_1)$	18.601	58.478	----	16.218
$Lp(X_1) \rightarrow \sigma^*(P-O_2)$	79.211	----	----	103.706
$Lp(N_1) \rightarrow \sigma^*(P-O_2)$	12.582	----	14.254	16.678
$Lp(O_2) \rightarrow \sigma^*(P-N_1)$	39.124	----	38.999	----
$Lp(O_2) \rightarrow \pi^*(P=X_1)$	17.430	----	21.694	----

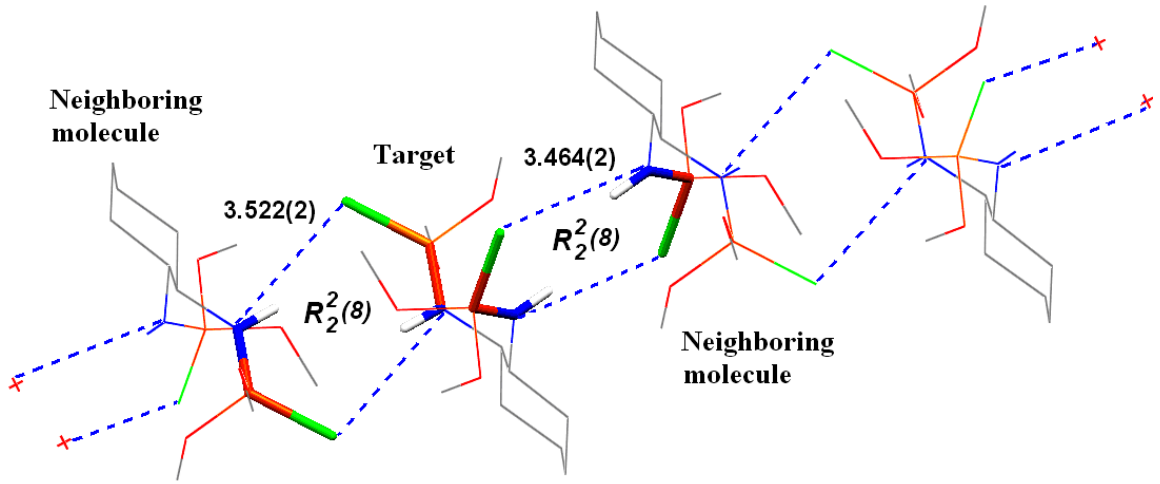
Neighboring molecule
Target
3.522(2)
3.464(2)
$R_2^2(8)$
$R_2^2(8)$
Neighboring molecule

Fig. 1.

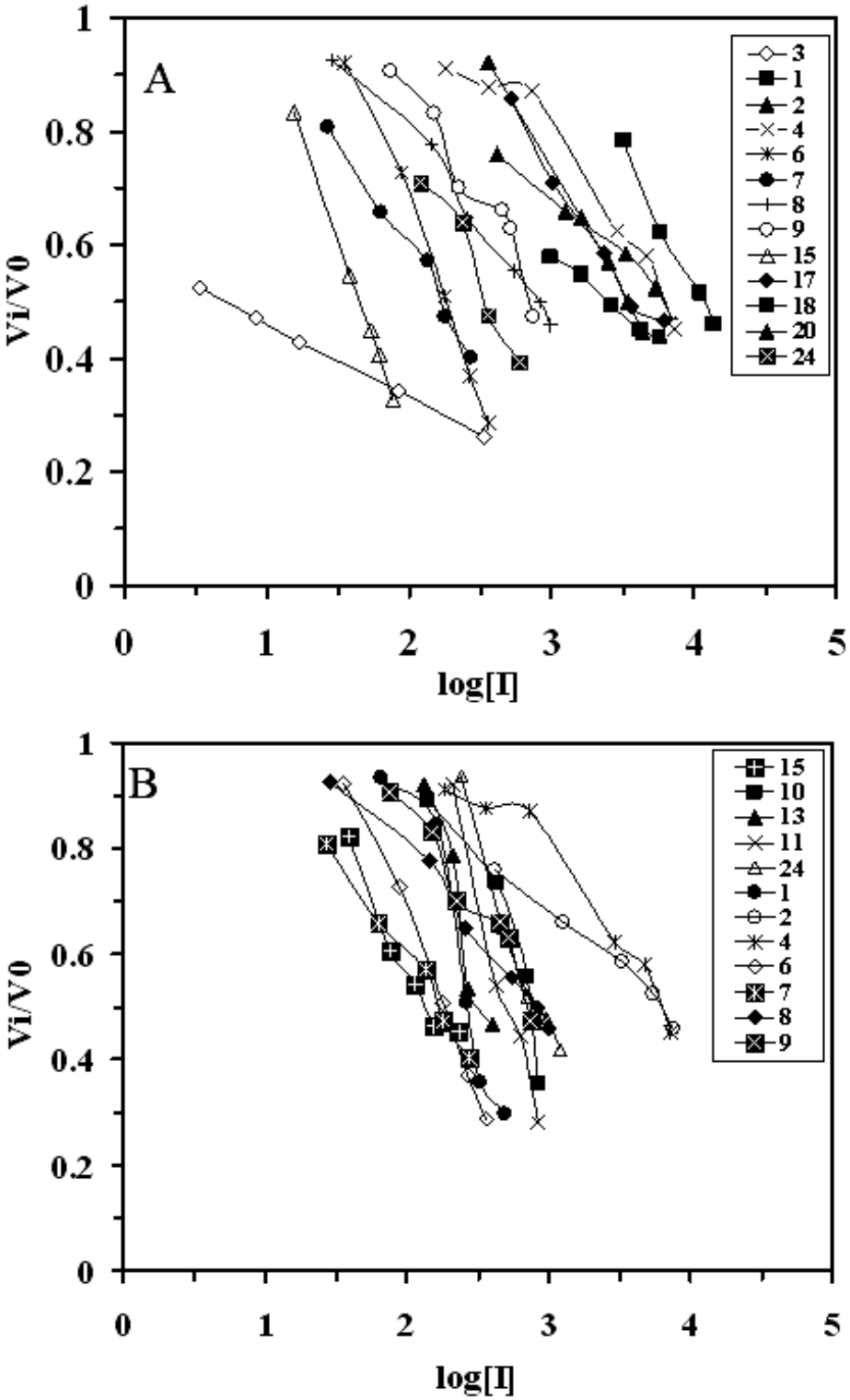
A
Vi/V0
log[I]
3
1
2
4
6
7
8
9
15
17
18
20
24
B
Vi/V0
log[I]
15
10
13
11
24
1
2
4
6
7
8
9

Figure 2.

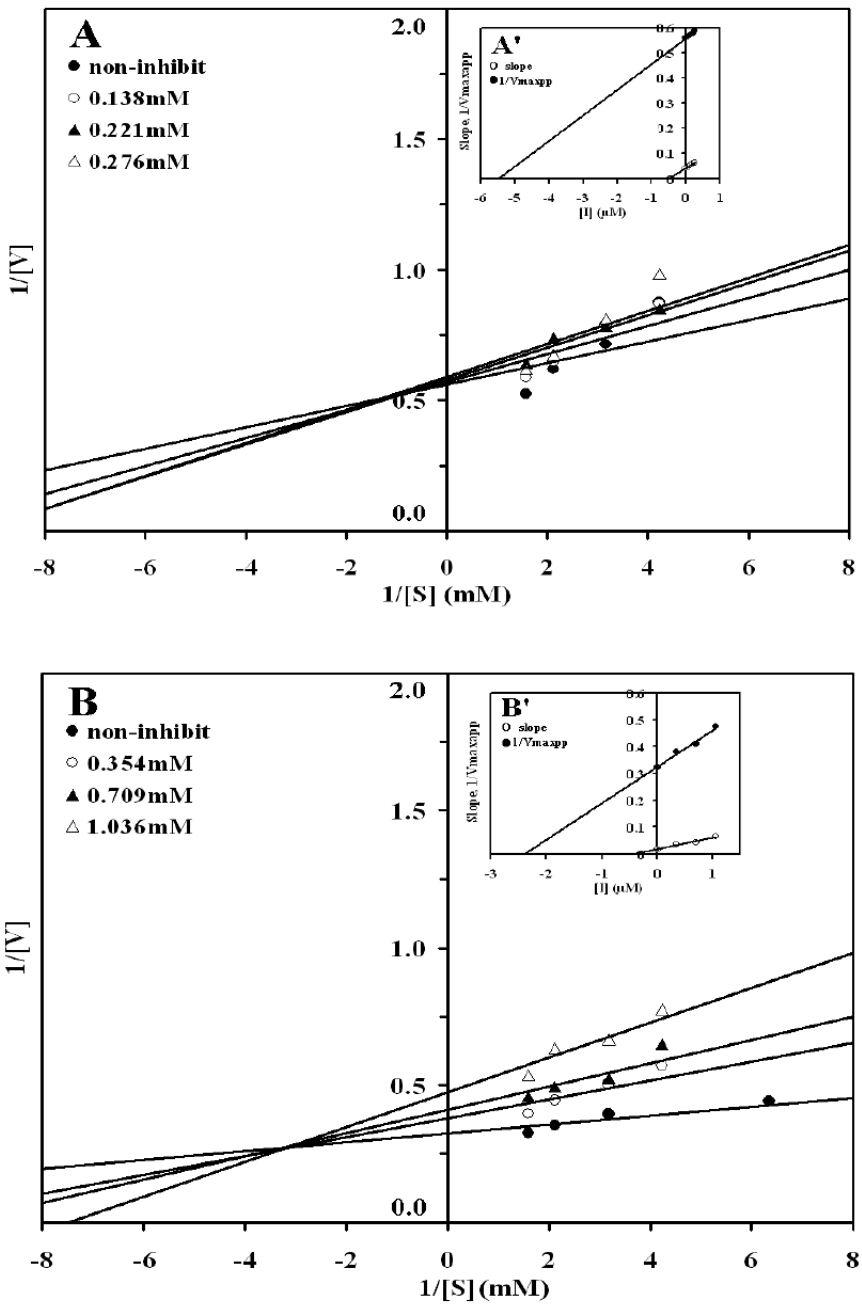
A
non-inhibit
0.138mM
0.221mM
0.276mM
1/[V]
1/[S] (mM)
A'
slope
1/Vmaxapp
Slope, 1/Vmaxapp
[I] (μM)
B
non-inhibit
0.354mM
0.709mM
1.036mM
1/[V]
1/[S] (mM)
B'
slope
1/Vmaxapp
Slope, 1/Vmaxapp
[I] (μM)

Figure 3.

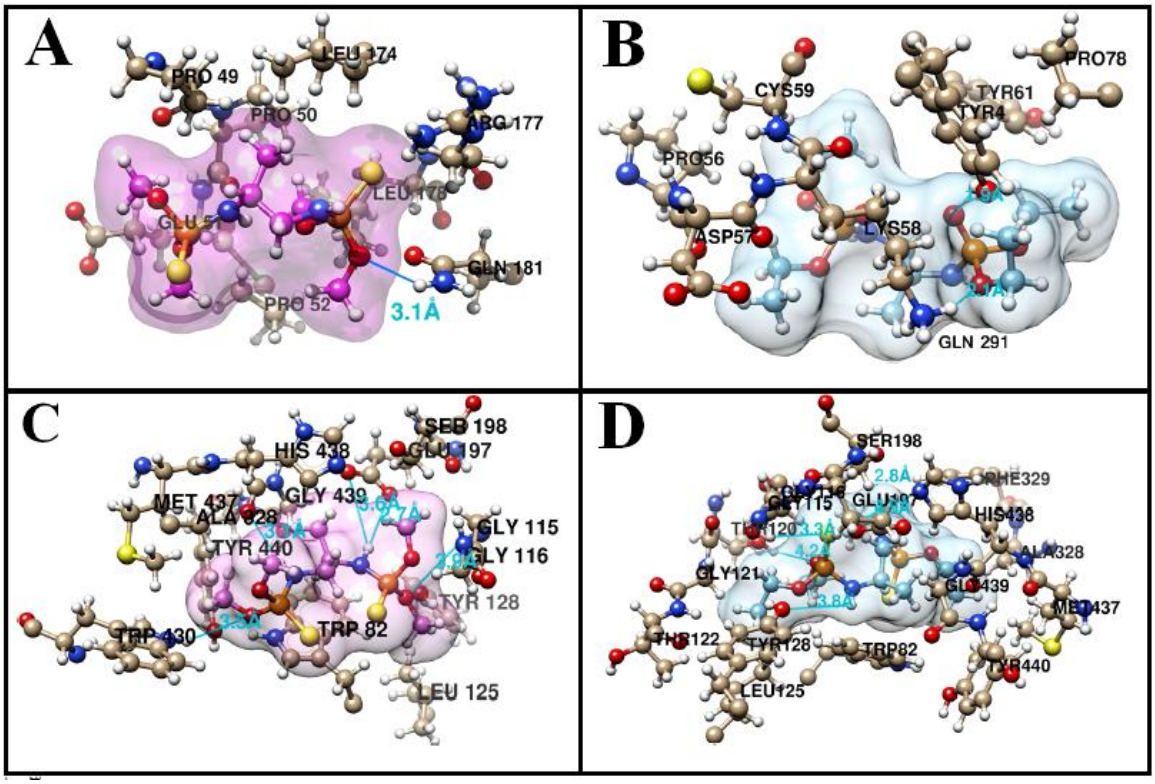
A
PRO 49
LEU 174
PRO 50
ARG 177
LEU 178
GLU 51
GLN 181
PRO 52
3.1Å
B
PRO78
CYS59
TYR61
TYR4
PRO56
ASP57
LYS58
GLN 291
C
SER 198
HIS 438
GLU 197
MET 437
GLY 439
ALA 328
TYR 440
GLY 115
GLY 116
TYR 128
TRP 430
TRP 82
LEU 125
D
SER198
PHE329
GLY116
GLY115
GLU197
HIS438
THR120
ALA328
GLY121
GLU439
MET437
THR122
TYR128
TRP82
TYR440
LEU125

Figure 4.

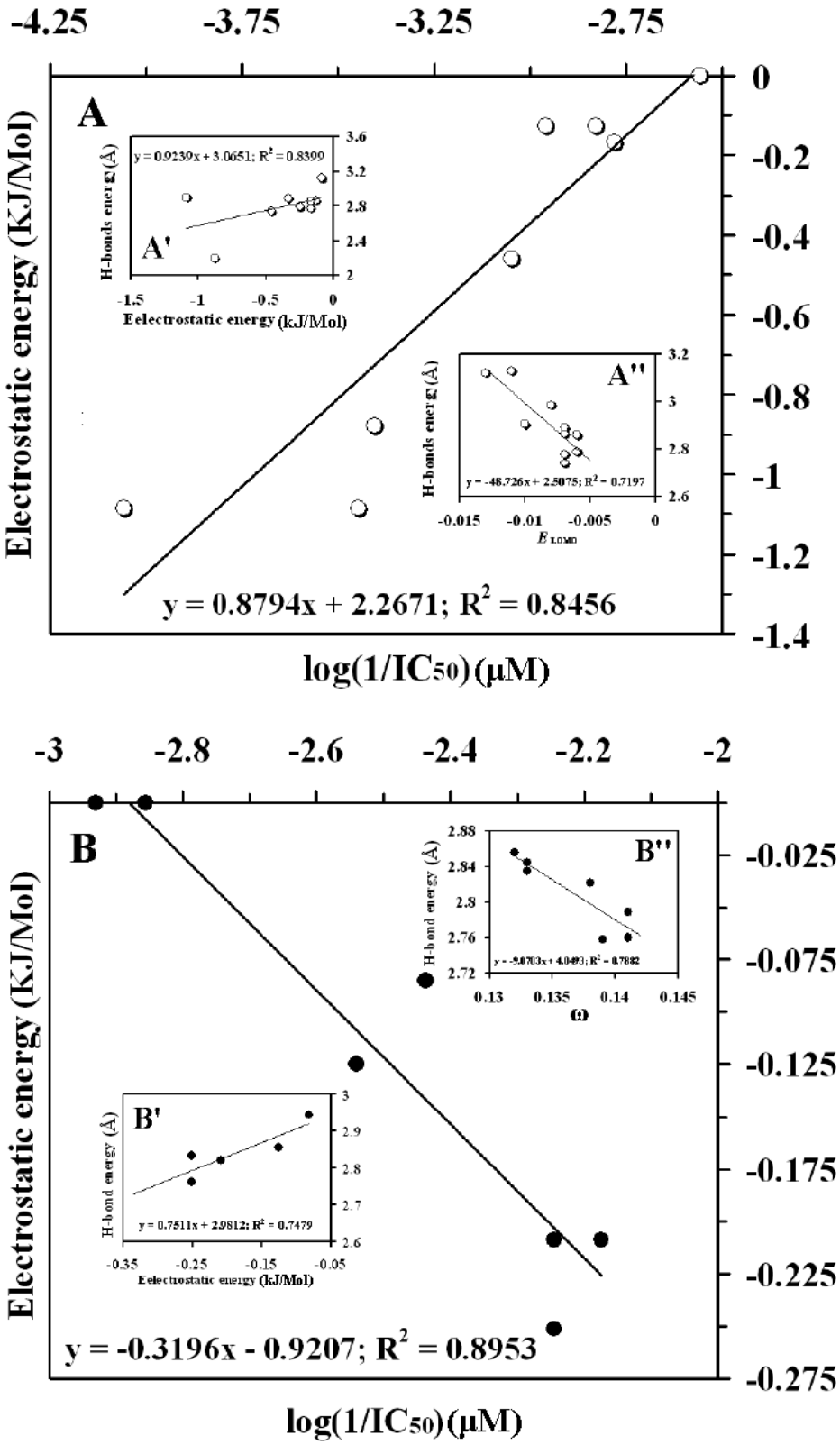
A
y = 0.8794x + 2.2671; R² = 0.8456
Electrostatic energy (KJ/Mol)
log(1/IC50) (μM)
A'
y = 0.9239x + 3.0651; R² = 0.8309
H-bonds energy (Å)
Electrostatic energy (kJ/Mol)
A''
y = -48.726x + 2.5075; R² = 0.7197
H-bonds energy (Å)
B
y = -0.3196x - 0.9207; R² = 0.8953
Electrostatic energy (KJ/Mol)
log(1/IC50) (μM)
B'
y = 0.7511x + 2.9812; R² = 0.7479
H-bond energy (Å)
Electrostatic energy (kJ/Mol)
B''
y = -9.0703x + 4.0493; R² = 0.7882
H-bond energy (Å)
ω

Figure 5.

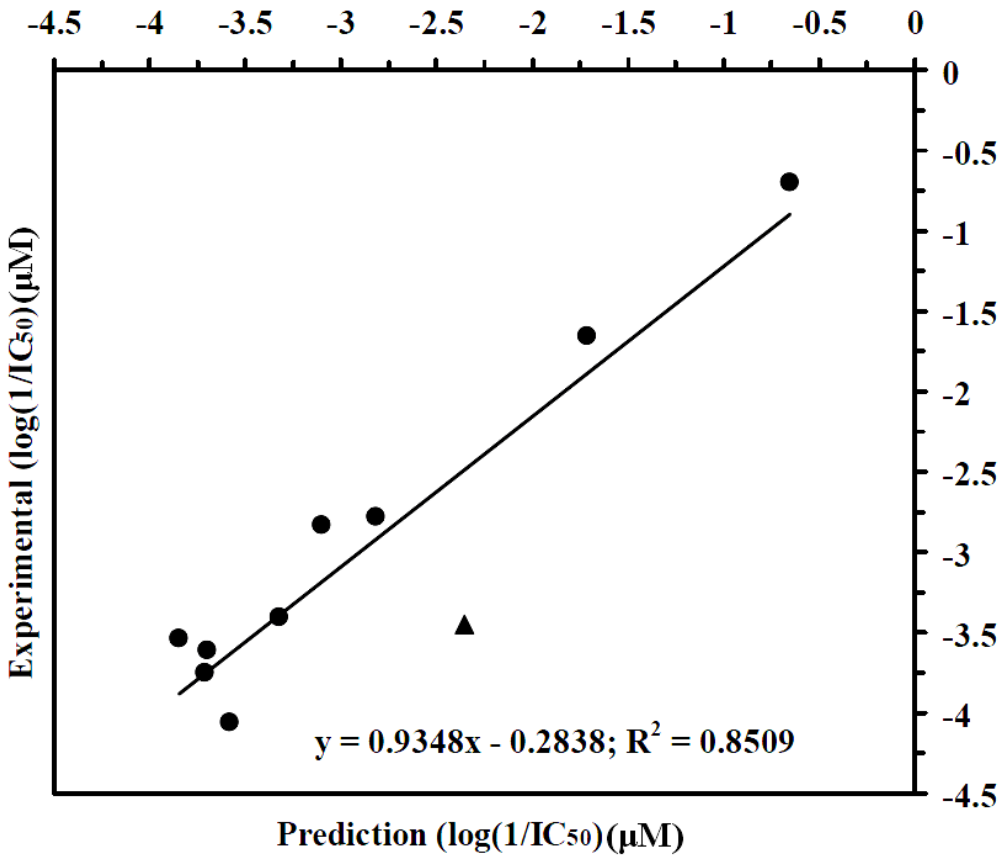
-4.5
-4
-3.5
-3
-2.5
-2
-1.5
-1
-0.5
0
Experimental (log(1/IC50)(μM)
Prediction (log(1/IC50)(μM)
y = 0.9348x - 0.2838; R2 = 0.8509

Figure 6.

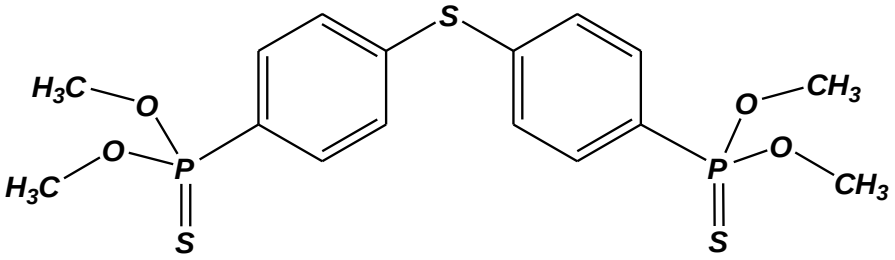

Scheme 1.

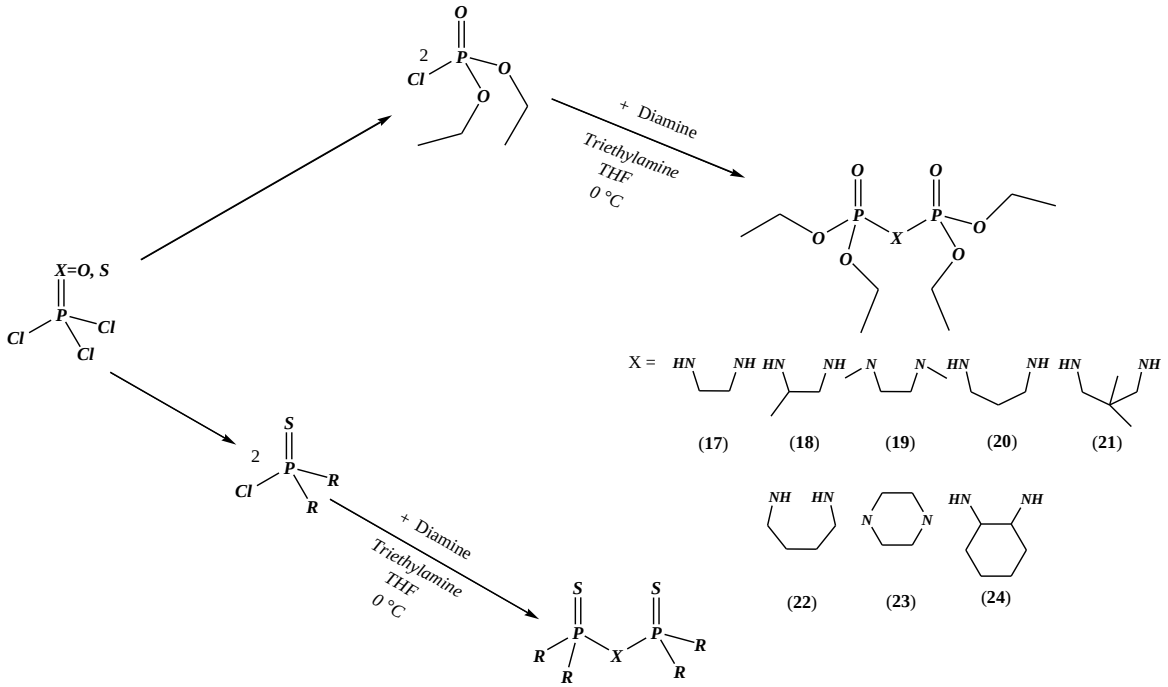

$R = OCH_3$; $X = NH\text{-}(CH_2)_2\text{-}NH$ (**1**), $NH\text{-}CH(CH_3)\text{-}CH_2\text{-}NH$ (**2**), $N(CH_3)\text{-}(CH_2)_2\text{-}(CH_3)N$ (**3**), $NH\text{-}(CH_2)_3\text{-}NH$ (**4**), $NH\text{-}CH_2\text{-}C(CH_3)_2\text{-}CH_2\text{-}NH$ (5), $NH\text{-}(CH_2)_4\text{-}NH$ (**6**), $N(CH_2)_4N$ (**7**), $N(CH_2)_5N$ (**8**), $NH\text{-}(C_6H_{10})\text{-}NH$ (**9**)

$R = OC_2H_5$, $X = NH\text{-}(CH_2)_2\text{-}NH$ (**10**), $NH\text{-}CH(CH_3)\text{-}CH_2\text{-}NH$ (**11**), $N(CH_3)\text{-}(CH_2)_2\text{-}(CH_3)N$ (**12**), $NH\text{-}(CH_2)_3\text{-}NH$ (**13**), $NH\text{-}CH_2\text{-}C(CH_3)_2\text{-}CH_2\text{-}NH$ (**14**), $N(CH_2)_4N$ (**15**), $NH\text{-}(C_6H_{10})\text{-}NH$ (**16**)

Scheme 2.